Journal of Nanobiotechnology

RESEARCH

Open Access

Youthful small extracellular vesicles restore the function and reparative capacity of inflammatory-impaired periodontal ligament stem cells via delivering protein biglycan for bone regeneration

Jiaqi Yang[1,2†], Junxiang Su[1,2,3†], Zhuo Sun[1,2], Yeqing Song[2], Yimei Zhang[4], Ziqian Zhang[1,2], Jizhen Wei[1,2], Xin Shi[5*], Nan Jiang[2*] and Xuejun Ge[1*]

Abstract

Regenerating inflamed bone defects represents a severe clinical challenge due to the undesirable inflammatory microenvironment. The inflammatory stimulus poses a weighty threat to the regenerative capacity of endogenously derived mesenchymal stem cells (MSCs), which are mainly responsible for osteogenic differentiation, thereby resulting in compromised endogenous bone formation. Consequently, alleviating the biological characteristics of inflammatory-impaired MSCs is crucial for promoting inflamed bone regeneration. Nano-sized small extracellular vesicles (sEVs) have emerged as promising therapeutic tools to orchestrate MSCs fate due to their intrinsic biocompatibility and encapsulated bioactive contents. In the present study, we extracted sEVs from youthful and adult dental pulp MSCs and explored their ability to recover inflammation-compromised periodontal ligament stem cells (IPDLSCs). The results indicated that both types of sEVs were capable of facilitating IPDLSCs osteogenesis. However, young sEVs exhibited a more robust potential at a lower concentration compared to adult sEVs. Mechanically, young sEVs enhanced the expression of bone morphogenetic protein 4 (BMP4) via delivering the protein Biglycan, which correspondingly promoted the osteogenic capability of IPDLSCs. Collectively, our findings emphasized that young sEVs hold enormous potential to rescue the inherent function and regenerative competence of inflammation-impaired MSCs, shedding light on their promising therapeutic prospects for infected bone regeneration.

†Jiaqi Yang and Junxiang Su contributed equally.

*Correspondence:
Xin Shi
shixin@tjh.tjmu.edu.cn
Nan Jiang
nanjiang@bjmu.edu.cn
Xuejun Ge
gxj19722003@163.com

Full list of author information is available at the end of the article

Keywords Youthful sEVs, Inflamed mesenchymal stem cells, Biglycan, Osteogenesis, Infectious bone defects

Introduction

Infectious bone defects, characterized by the partial or massive loss of bone tissue resulting from contamination diseases [1], remain one of the severe challenges in regenerative treatments because of the high refractory rate [2]. An ideal treatment strategy for inflammatory bone defects should achieve two critical objectives, namely eliminating inflammatory responses and inducing bone regeneration. However, currently prevalent clinical practices involving conservative surgical procedures or mechanical treatments are primarily dedicated to eradicating necrotic tissue or cells from the lesion site. The local administration of antibiotics or antimicrobial agents, on the other hand, is mainly aimed at reestablishing microbial homeostasis and inhibiting the development of inflammation [3]. In this regard, conventional treatment strategies neglect the restoration of the biological properties of inflammatory MSCs [4]. It is worth noting that bone regeneration largely depends on the osteogenic ability of endogenously derived MSCs. Notably, the functional restoration of compromised stem cells was confronted with multiple obstacles in an inflammatory environment, which adversely posed a suppressive effect on endogenous bone regeneration [5].

As a common clinical oral disease, periodontal bone defects encompass various chronic inflammatory conditions of the periodontal ligament, cementum, and alveolar bone caused by periodontitis, apical periodontitis, or trauma [6]. Despite recent considerable advancements in periodontal therapy, regenerating infected alveolar bone remains a major clinical challenge. Periodontal ligament stem cells (PDLSCs) have been identified to possess multilineage differentiation capability and play crucial roles in periodontal alveolar bone regeneration [7]. Increasing evidence has verified that the osteogenesis function of PDLSCs is detrimentally impaired in chronic inflammatory microenvironment, which is mediated by proinflammatory cytokines, deubiquitinating enzymes and other factors [8, 9]. Hence, orchestrating the differentiation fate commitment of inflammatory PDLSCs (IPDLSCs) and rescuing their compromised osteogenic potential have emerged as essential goals for infected bone regeneration therapy.

Small extracellular vesicles (sEVs), nanoscale vesicles (30–150 nm) released by nearly all cell types, have been extensively employed as novel diagnostic biomarkers and targeted drug delivery tools for treating various diseases in nano-biomedical fields [10, 11]. In contrast to artificial nanoparticles, sEVs are efficient in entering recipient cells with targeted accumulation and minimal immune clearance upon exogenous administration [12]. Similar results can be observed in cell membrane-camouflaged nanoparticles [13]. EVs can mediate intercellular communication by transferring a wide range of bioactive molecules, such as lipids, proteins, DNA, mRNAs, and microRNAs, and serve diverse and pivotal roles in different pathophysiological microenvironments [14]. Moreover, the contents and functions of sEVs are intimately associated with the types of parental cells [15]. However, representing a crucial influencing factor, aging contributes to a multitude of physiological changes in parent cells at molecular and cellular levels, thus resulting in versatile alterations of sEVs biological characteristics [16]. As recently reported work, youthful sEVs secreted by young bone marrow MSCs exerted higher potential to reduce M1 microglial polarization, which suggested that stem cell aging elicited negative impact on sEVs function and their therapeutic value [17]. In particular, compared with adult dental pulp stem cells (DPSC) originating from human permanent teeth, dental pulp stem cells from human exfoliated deciduous teeth (SHED) are recognized as relatively much younger and more vigorous mesenchymal stem cells originated from dental pulp MSC [18]. Notably, while maintaining the typical characteristics of MSCs, SHED have been elucidated to exhibit more desirable properties, especially considering their beneficial effect on tissue regeneration and inflammation suppression. Accumulating research has illuminated that SHED can promote the repair and regeneration of damaged tissues through paracrine mechanisms, laying a solid foundation for the clinical translation of tissue engineering [19]. In line with this, sEVs derived from SHED (SHED-sEVs) have also been acknowledged as promising novel therapeutic approaches for autoimmune disorder [20], acute inflammation [21], periodontitis [22] and pulp regeneration [23]. However, it remains elusive whether SHED-sEVs can reconstitute and recover the normal biological status of inflammation-impaired MSCs, thus expanding their therapeutic application.

In the current study, we confirmed that young SHED-sEVs could efficiently alleviate the function and regenerative capability of PDLSCs subjected to chronic inflammatory environments through the delivery of the protein Biglycan, which targeted BMP4 signaling pathway. Utilizing apical periodontitis and massive bone defect as disease models, we demonstrated that young SHED-sEVs as novel promising therapeutic tools hold enormous potential for inflammatory bone regeneration.

Materials and methods

Cell culture and siRNA transfection

Stem cells from human exfoliated deciduous teeth (SHED) and dental pulp stem cells (DPSC) were obtained from Oral STEM CELL BANK of Beijing, Tason Biotech Co., Ltd and cultured in DMEM medium (Gibco, Thermo Fisher Scientific, USA) supplemented with 10% (v/v) FBS (Cytiva Hyclone, Australia) and 1% (v/v) P/S (Gibco). PDLSCs were purchased from Wuhan Pricella Biotechnology Co., Ltd. and cultured in DMEM medium supplemented with 10% (v/v) FBS and 1% (v/v) P/S. IPDLSCs were harvested from the periodontal tissue of extracted teeth according to clinical examination with the diagnosis of periodontitis or chronic apical periodontitis at Shanxi Medical University Hospital of Stomatology. The study protocol was approved by the Ethics Committee of Shanxi Medical University School and Hospital of Stomatology approval (2023SJL15). After teeth extraction, granulation tissues in the alveolar fossa were scraped and were placed in sterile PBS. In clean bench, the granulation tissues were cut into small pieces, and were digested with 0.25% trypsin for 5 min at 37 ℃. Subsequently, the reaction was immediately terminated using culture medium. DMEM containing 20% fetal bovine serum and 1% penicillin/streptomycin antibiotics (P/S) was added to tissue blocks which were incubated in a 5% CO_2 incubator at 37 ℃. When cells fuse to 90%, they were passaged and incubated in DMEM supplemented with 10% (v/v) FBS and 1% (v/v) P/S.

When cells density reached 80%, SHED was transfected as follows. According to the manufacturer's requirements, siRNA (BIOSYNTECH, China) with concentrations as 5 nM or 10 nM, and CALNP™ RNAi (D-Nano) were used as the transfection reagent. After 24 h of transfection, total RNA was extracted, and total protein was extracted after 48 h.

Cell proliferation analysis

The proliferation ability of cells was evaluated using Cell Counting Kit-8 (CCK-8). Each well of the 96 well plate was inoculated with 2000 cells. After 8 h of cultivation, cells were incubated with CCK-8 and the absorbance value was measured at 450 nm by a spectrometer, which was used as the starting point for daily testing at the same time. IPDLSCs were processed with SHED-sEVs and DPSC-sEVs with the concentration of 1 μg/mL and 10 μg/mL and were co-cultured for another 4 days.

Flow cytometry

PDLSCs and IPDLSCs were harvested at passage 3–7. Fluorescein isothiocyanate (FITC)-conjugated antibodies against CD45; phycoerythrin-conjugated antibodies against CD146 and CD29 were obtained from BD Pharmingen. Allophycocyanin-conjugated antibodies against CD44 were obtained from Proteintech. Phycoerythrin-conjugated antibodies against CD90 and CD105 were obtained from Biolegend. Antibodies were diluted at a 1:50 ratio with PBS and then were added to the cell resuspension and incubated for 30 min in dark. After washing with PBS and centrifugation, cells were resuspended with 500 μl PBS and were tested on the Accuri-C6 (BD Bioscience).

Preparation of cells derived sEVs

DPSCs and SHEDs at passages 3–7 were cultured to in a serum-free DMEM medium and 1% penicillin/streptomycin for 24 h and the supernatants was collected. The supernatant was centrifuged at 300 x g for 10 min, 2,000 x g for 10 min, and 10,000 x g for 30 min, respectively, to get rid of dead cells, cell debris and macromolecular vesicle. Supernatant was filtered by 0.22 μm filter (Millipore, USA) to elucidate microvesicles. After that, the supernatant was transferred into an ultrafiltration tube, and was centrifuged at 100,000 x g for 70 min at 4 ℃ [14]. Then the sEVs were dissolved by PBS. The morphology and size of extracted DPSC-sEVs and SHED-sEVs were examined with transmission electron microscopy (JEM-1400, Japan) and ZetaView (Particle Metrix, German). Specific extracellular vesicle markers were inspected using Western blotting.

Uptake of sEVs

Purified DPSC or SHED derived sEVs were labeled with PKH26 fluorescent labeling kit (Sigma, MO, USA) as previously reported [24]. Briefly, 2 μM PKH26 was mixed with sEVs for 4 min and then washed five times using a 100-kD filter (Millipore) to remove excess dye. Labeled sEVs were harvested by using an sEVs isolation reagent (Invitrogen) according to the manufacturers' instructions. Then labeled DPSC-sEVs and SHED-sEVs were added to the cell culture medium at a concentration of 1 μg/mL. After incubation for 6 and 12 h, samples were collected. After fixation with 4% paraformaldehyde, phalloidin was added and incubated at room temperature for 30 min. To assess sEVs colocalization with lysosomes, PKH26-labeled DPSC-sEVs and SHED-sEVs were incubated with IPDLSCs for 12 h at a concentration of 1 μg/mL and then fixed with 4% paraformaldehyde. IPDLSCs were permeabilized and stained with the lysosome membrane marker LAMP1 (cellsignal, 1:300), followed by FITC-labeled secondary antibodies. Finally, cells were sealed in a sealing solution containing DAPI and examined using a under laser confocal microscopy (Zeiss). The colocalization rate of sEVs and lysosomes was measured using the ImageJ software as previously described [25, 26].

Proteomics analysis of sEVs

DPSC-sEVs and SHED-sEVs were collected in three groups each, and each sample was prepared independently for protein enzymatic hydrolysis. DIA (Data Independent Acquisition) qualitative and quantitative analysis was performed. The volcano plot of protein expression differences and t-test between DPSC-sEVs and SHED-sEVs samples were plotted. The differentially expressed proteins between groups were analyzed using hierarchical clustering algorithm and were presented in heatmaps. Among them, the screening criteria were that the expression of differentially expressed proteins changed by more than 1.5 times and $p < 0.05$. All differentially expressed proteins were annotated with Gene Ontology (GO), and were subjected to GO enrichment analysis using Fisher's exact test to reveal the overall functional enrichment characteristics of differentially expressed proteins.

Osteogenic assays

For osteogenic induction in vitro, 1×10^5 IPDLSCs were incubated overnight in 24-well dishes. While replacing with osteogenic medium, IPDLSCs were stimulated with DPSC-sEVs and SHED-sEVs at the concentration of 1 μg/mL or 10 μg/mL, respectively. For the activity of alkaline phosphatase, different concentrations of DPSC-sEVs and SHED-sEVs were added to cells for osteogenic induction for 7 days. After 7 days of osteogenic culture, Alkaline phosphatase (ALP) staining was performed using BCIP/NBT Alkaline Phosphatase Color Development Kit (Beyotime). To quantify alkaline phosphatase activity, 500 μL of p-NPP solution was added and incubated in dark for no more than 3 min. The cells were measured by reading the absorbance at 405 nm in triplicate using multifunctional enzyme marker. After 21 days of osteogenic culture, cells were fixed with 4% paraformaldehyde fix solution for 30–60 min. 1% Alizarin Red (ARS) staining solution was incubated at room temperature on a shaker for 30 min. Mineralized nodules were scanned and photographed under microscope. For quantification, 10% cetylpyridinium chloride was added to the well plate and measured by reading the absorbance at 562 nm using spectrophotometer and were conducted quantitative analysis.

Quantitative real-time polymerase chain reaction (qRT-PCR) analysis

The total RNA of cells was extracted using TRIzol reagent (Invitrogen), which were reverse transcribed into cDNA using PrimeScript™ RT Master Mix (TaKaRa). According to the manufacturer's requirements, SYBR Green Master (mix) (Roche), primers, cDNA, and DEPC were mixed proportionally for quantitative PCR on a 7500 Real Time PCR System (Applied Biosystems). The relevant primer sequences are listed in Supplementary Tabel 1. Using the expression level of GAPDH as an internal reference, experimental data were calculated the mean and standard deviation based on three independent experiments.

Western blot

The total protein of sEVs or cells were extracted using RIPA lysis solution. After proteins denatured, samples were separated using SDS-PAGE gel and were transferred onto PVDF membranes (Millipore). Proteins were blotted with antibodies to rabbit GAPDH (1:5000, Proteintech), CD63 (1:500, Abcam), CD81 (1:1000, Proteintech), Tsg101 (1:1000, Abcam), ALP (1:400, Abcam), OCN (1:500, Abcam), RUNX2 (1:500, Abcam), BMP4 (1:500, Signalway), Biglycan (1:400, Proteintech). Goat anti-rabbit IgG secondary antibody was purchased from ZSGB-Bio. Membranes were exposed and photographed in the FX gel imaging system (VILBR). After exposure, each group of cells was measured the grayscale values of the bands, and was analyzed the relative expression levels of the target gene proteins with IMAGEJ software.

Animal models and tissue preparation

Male 7–8 weeks old Sprague-Dawley rats were purchased from Beijing Vital River Laboratory Animal Technology Co., Ltd. and our experiments were conducted in the central laboratory of Peking University Stomatology Hospital and were supervised by the Animal Use and Care Committee of Peking University Health Science Center (LA2021036). Rats are kept in a specific-pathway-free animal Laboratory with constant water and feed.

1) Fabrication and release of sEVs and hydrogel scaffolds.

First, Heprasil, Gelin-S, and Extralink(Advanced Biomatrix, Carlsbad, CA)were prepared in a 1: 1: 0.5 ratio. DPSC-sEVs and SHED-sEVs, labeled with PKH26 as previously described, were added to the scaffolds at the final concentration was adjusted to 20 μg/mL, and then co-cultured at 37 ℃ for 1 h. To observe the distribution of sEVs, the hydrogel scaffolds were scanned with the LSM 4 EXCITER confocal laser microscope (Zeiss).

2) Establishment and treatment of rat models of periapical periodontitis.

Thirty 7–8 weeks old rats were adapted for 1 week before surgeries. Animals were anesthetized by intraperitoneal injection of pentobarbital sodium. The distal buccal root canal of the maxillary first molar was exposed using ball drills and exposed for 21 days as previously described [27]. When the area of apical inflammation was stable, the root canal was cleared with root canal

files, and SHED-sEVs and DPSC-sEVs were injected into the root canal with microinjectors. The root canal was sealed temporarily with glass-ionomer cement and sEVs were injected through the root canal per week. After two weeks, the maxillas were harvested for H&E staining and immunohistochemistry.

3) Establishment and treatment of rat models of infectious alveolar bone defect.

Twenty-four rats were anesthetized pentobarbital sodium anesthesia, a defect of 3 mm diameter and 1 mm depth was created in the apical area of the first mandibular molar using a ball drill to simulate periapical inflammation. Subsequently, rinse the defect area with physiological saline and inject 10 μg of LPS and LTA into the defect area respectively. Animals were assigned to four groups randomly: (1) untreated (blank group), (2) hydrogel, (3) DPSC-sEVs+hydrogel, (4) SHED-sEVs+hydrogel. After this process, the hydrogel, DPSC-sEVs+hydrogel and SHED-sEVs+hydrogel was respectively placed at the apical defect site. In 14 days post-operatively, the rats were euthanized with carbon dioxide. Then, the right mandibular bones were collected from rats and performed CT scanning and staining.

4) Micro-CT.

The bone samples from Sprague-Dawley rats were fixed in 4% paraformaldehyde and scanned by Micro-CT (Siemens) with a resolution of 20 μm. Three-dimensional reconstruction and quantitative analysis were conducted using Inveon Research Workplace software with analysis indicators including percentages of bone volume/total volume (BV/TV) and bone mineral density (BMD).

5) Histological and morphological staining.

After fixing, samples were immersing in 10% EDTA decalcification solution for two weeks. After embedding in paraffin, samples were cut with a thickness of 5 μm. Sections were analyzed for hematoxylin and eosin (HE), Masson's trichrome staining and immunohistochemistry. For immunohistochemistry, sections were subjected to conventional dewaxing and hydration methods, followed by antigen repair, and incubated at room temperature in the dark using endogenous peroxidase inhibitors (ZSGB-BIO, Cat# PV-9001). Then, the sections were nonspecifically blocked by 5% bovine serum albumin (BSA, Solarbio), and incubated with the primary antibody BMP4 (1:250, Abcam), Runx2 (1:400, CST) overnight at 4 ℃. On the second day, sections were washed for three times with PBS, and the samples were incubated at room temperature in sequence with polymer Helper (ZSGB-BIO) and poly-HRP-anti-Rabbit IgG (ZSGB-BIO). Finally, the samples were colored using DAB reagent kit (ZSGB-BIO) and sealed with neutral resin.

Statistical analysis

All quantitative data were analyzed using SPSS and expressed as mean ± standard deviation (SD). The comparison between two groups was conducted using a t test. Multiple comparisons between groups were conducted using one-way ANOVA or two-way ANOVA, followed by Tukey's post hoc. A value of $P<0.05$ indicates a significant difference statistically.

Results

Identification of young and adult dental pulp MSCs derived sEVs

First, we harvested SHED-sEVs and DPSC-sEVs by virtue of ultracentrifugation methods, and it was identified by transmission electron microscopy (TEM) examination that both SHED-sEVs and DPSC-sEVs exhibited a typical cup-shaped morphology (Fig. 1A, left panel), and no notable difference in shape was observed between them. Besides, as suggested by nanoparticle track analysis (NTA), SHED-sEVs possessed a similar size distribution to DPSC-sEVs, ranging from nm to nm, with an average diameter of around 110 nm (Fig. 1A, right panel). In addition, western blot (WB) confirmed that both types of sEVs are positive for transmembrane proteins CD63 and CD81 and cytoplasmic protein TSG101 (Fig. 1B), indicating that SHED-sEVs and DPSC-sEVs satisfied the criteria of sEVs. Then, focused on the role of SHED-sEVs in cellular functions, we performed an uptake assay, and it was depicted that DPSC-sEVs and SHED-sEVs positively stained by PKH26 (red fluorescence) could be effectively internalized by IPDLSCs with time elapse and scattered between cytoplasmic membranes (Fig. 1C), providing a theoretical basis for mediating IPDLSC behaviors. In addition, we verified whether sEVs may escape from lysosomes after cellular uptake. A small fraction of SHED-sEVs and DPSC-sEVs were observed to colocalize with lysosome marker LAMP1 (Sup Fig. 1a), and quantitative analysis indicated that the colocalization percentage with Lamp-1 to be 16.1% and 17.8%, respectively (Sup Fig. 1b). Of importance, no difference was noted between these two types of sEVs. In light of this, we clarified that SHED-sEVs and DPSC-sEVs regulated the proliferative property of IPDLSCs in a dose- and time-dependent manner (Fig. 1D). Of importance, when exposed to 1 μg/mL of DPSC-sEVs, IPDLSC showed a remarkably enhanced proliferation at 24 h and 48 h. On the opposite, 10 μg/mL of SHED-sEVs exerted a robust promoting effect on IPDLSC proliferation after being treated for 24 h. This possibly could be explained by different bioactive contents that SHED-sEVs and DPSC-sEVs shuttled. As a consequence, we employed two concentrations

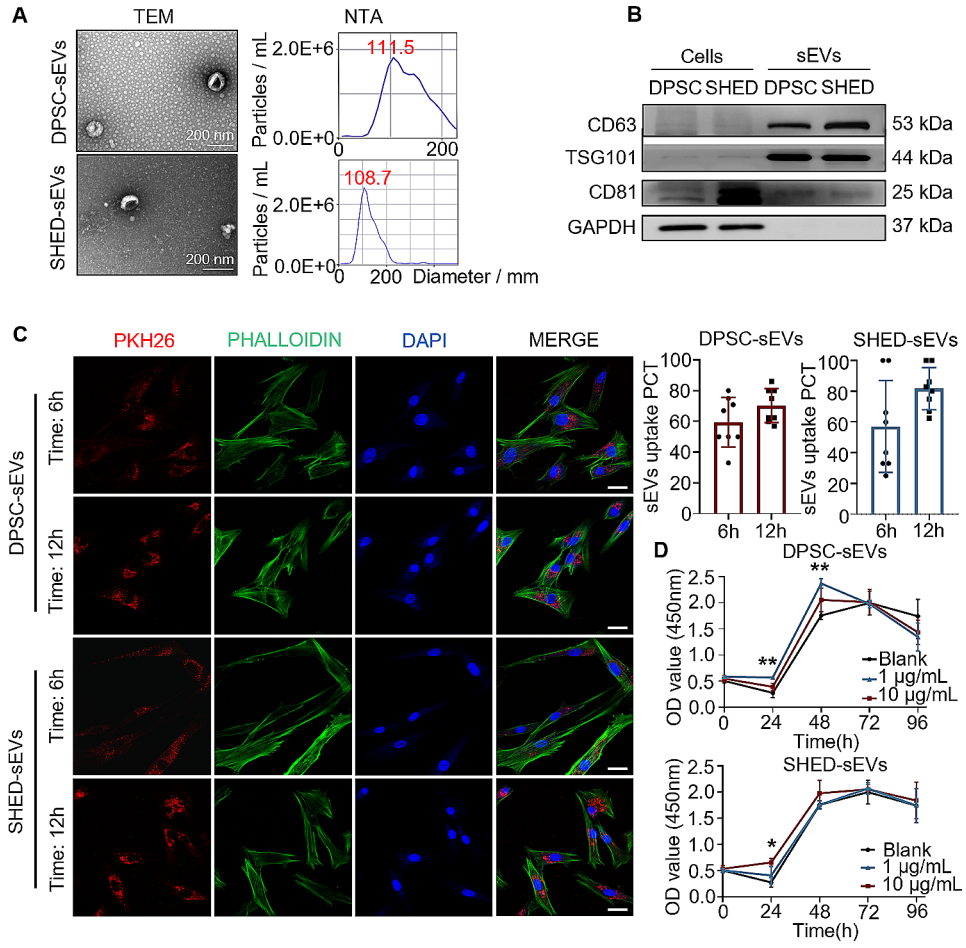

Fig. 1 The characterization of DPSC-sEVs and SHED-sEVs and impacts on the proliferation of PDLSCs and IPDLSCs. (**A**) As assessed by TEM and NTA, DPSC-sEVs and SHED-sEVs displayed characteristic attributes of sEVs in terms of morphology, size distribution. Scale bar, 200 nm. (**B**) The presence of sEVs typical protein markers, including tetraspanins CD63 and CD81 and cytosolic protein TSG101, was consistently identified in DPSC-sEVs and SHED-sEVs through WB detection. (**C**) As clarified by immunofluorescence staining, DPSC-sEVs and SHED-sEVs positively stained by PKH26 (red fluorescence) could be taken up by IPDLSCs and scattered between cytoplasmic membranes (green fluorescence) and nuclei (blue fluorescence). Scale bar, 50 μm. (**D**) CCK-8 assessment depicted that DPSC-sEVs and SHED-sEVs could regulate the proliferative competency of IPDLSCs in a dose- and time-dependent manner. Data are presented as mean ± SD; One-way ANOVA was performed for comparisons. *$p < 0.05$, **$p < 0.01$

of sEVs, 1 μg/mL and 10 μg/mL, in the following research.

Young SHED-sEVs effectively restore IPDLSCs osteogenesis capability

To discover the effect of inflammatory environments on the characteristics of PDLSCs, IPDLSCs and healthy PDLSCs were isolated (Sup Fig. 2a). Then, IPDLSCs and PDLSCs were subjected to RT-PCR to evaluate the expression of inflammatory-related genes. Compared with PDLSCs, the expression of *IL-6*, *IL-1β*, and *TNF-α* were remarkably enhanced in IPDLSCs (Sup Fig. 2b). As revealed by the CCK-8 assay, IPDLSCs possessed a substantially higher proliferation potential than PDLSCs (Sup Fig. 2d). The above results preliminarily confirmed that the inflammatory stimulation contributed to the modification of PDLSC biological properties. However, by analyzing with flow cytometry, we demonstrated that PDLSCs and IPDLSCs shared similar expression profiles of MSC surface markers, and no significant difference was noted between them (Sup Fig. 2c).

To realize adequate periodontal bone regeneration under inflammatory circumstances, we paid immense attention to the multi-lineage differentiation capacity of IPDLSCs. Alizarin red staining demonstrated a considerably decrease in IPDLSCs (Fig. 2A), and only small punctate, scattered nodules could be identified. This was further ascertained by semi-quantification analysis. In accordance with these, inflammation exposure elicited an inhibitory effect on the expression of osteogenesis-associated mRNAs such as *BMP2*, *OCN*, and *Runx2* in IPDLSCs (Fig. 2B). Additionally, from the perspective of adipogenesis, IPDLSCs also

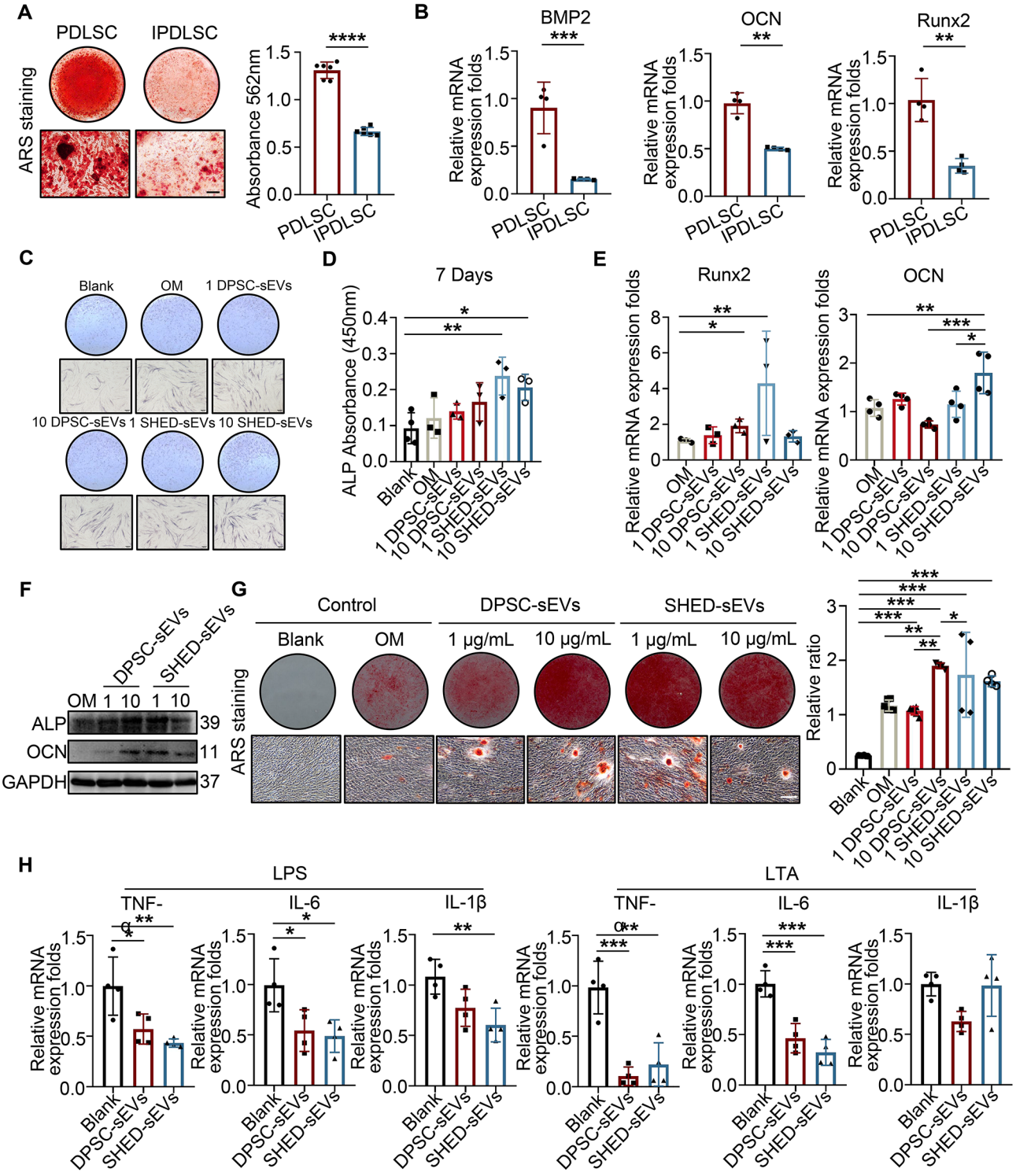

Fig. 2 DPSC-sEVs and SHED-sEVs at different concentrations modulate osteogenic and anti-inflammatory capabilities of IPDLSCs in vitro. (**A**) ARS staining revealed that osteogenesis of IPDLSC and PDLSC at 14 days, which was further validated by semi-quantification analysis. Scale bar, 200 μm. (**B**) According to RT-PCR, inflammatory stimulation elicited an inhibitory effect on the expression of osteogenesis-associated mRNAs such as BMP2, OCN, and Runx2 in IPDLSCs. (**C**) The employment of DPSC-sEVs and SHED-sEVs could facilitate ALP activity of IPDLSCs, and SHED-sEVs exhibited a much stronger potential than DPSC-sEVs as quantified in (**D**). (**E**) RT-PCR of the Runx2 and OCN mRNA expression of DPSC-sEVs and SHED-sEVs at 1 μg/mL and 10 μg/mL in IPDLSCs with osteogenesis culture. (**F**) WB results suggested that DPSC-sEVs and SHED-sEVs could potentiate the expression of ALP and OCN. (**G**) ARS staining of compared with DPSC-sEVs, SHED-sEVs at the different concentration of accumulation of calcified nodules in IPDLSCs. Scale bar, 100 μm. (**H**) RT-PCR showing the expression of TNF-α, IL-6 and IL-1β mRNA in IPDLSCs that had been pre-treated by LPS or LTA and then applied with SHED-sEVs, DPSC-sEVs or PBS for 12 h ($n=4$). Data are presented as mean ± SD; One-way ANOVA was performed for comparisons. *$p<0.05$, **$p<0.01$, ***$p<0.001$, ****$p<0.0001$

exhibited a compromised capacity to initiate adipogeneic differentiation, leading to decreased formation of lipid droplets (Sup Fig. 2e).

Subsequently, we aimed to investigate whether SHED-sEVs could rescue the osteogenic potential of IPDLSCs. Alkaline phosphatase (ALP) is crucial for mineral deposition and is commonly employed to indicate osteogenic differentiation. In our study, despite the fact that SHED-sEVs and DPSC-sEVs were capable of facilitating the ALP activity of IPDLSCs, SHED-sEVs possessed a much stronger potential than DPSC-sEVs (Fig. 2C, D). In accordance with the above results, SHED-sEVs and DPSC-sEVs have been detected to boost the expression of osteogenesis-associated mRNAs, including *Runx2* and *OCN* (Fig. 2E). Furthermore, in terms of protein level, WB results suggested that DPSC-sEVs and SHED-sEVs could potentiate the expression of ALP and OCN (Fig. 2F). In addition, as illustrated by alizarin red S (ARS) staining, the accumulation of calcified nodules in IPDLSCs was substantially promoted by SHED-sEVs and DPSC-sEVs. However, in contrast with 1 μg/mL of DPSC-sEVs, SHED-sEVs at the same concentration made a positive contribution to the promoted mineral deposition (Fig. 2G). Collectively, SHED-sEVs were proven to be more beneficial than DPSC-sEVs to orchestrate the osteogenic differentiation of IPDLSCs.

Next, we intended to figure out whether SHED-sEVs could attenuate the inflammatory state of IPDLSCs. Encouragingly, under inflammatory conditions induced by lipopolysaccharides (LPS) in vitro, as opposed to DPSC-sEVs that elicited no inhibitory effect, SHED-sEVs at 1 μg/mL held tremendous potential to inhibit pro-inflammatory gene levels in IPDLSCs (Fig. 2H). Furthermore, when subjected to lipoteichoic acid (LTA) stimulation in vitro, IPDLSCs exhibited a considerably reduced inflammatory performance after receiving DPSC-sEVs and SHED-sEVs, respectively (Fig. 2H). Regarding that LPS and LTA are major cell membrane constitutes in gram-negative bacteria and gram-positive bacteria, SHED-sEVs were more effective and dual-functional in attenuation of LPS- and LTA-induced inflammatory responses of IPDLSCs, shedding light on their amplified prospects in clinical translation. To sum up, our results identified the versatile roles of SHED-sEVs and emphasized that the application of lower dose of SHED-sEVs (1 μg/mL) could be developed as a promising approach compared to higher dose DPSC-sEVs in ameliorating the osteogenesis and suppressing the inflammation of IPDLSCs.

Young SHED-sEVs exhibit distinct proteins profiles

sEVs can transfer a variety of bioactive cargoes, such as proteins, lipids, DNA, mRNAs, and microRNAs to modulate the biological activities of recipient cells. To unveil ubiquitous proteins that governed the diverse functions of SHED-sEVs, we performed proteomic analysis. Hundreds of proteins were identified from SHED-sEVs and DPSC-sEVs (Fig. 3A). As illustrated by the volcano plot, 11 proteins were significantly differentially expressed in SHED-sEVs in comparison with DPSC-sEVs. Particularly, 4 proteins were upregulated, whereas 7 proteins were downregulated in SHED-sEVs. Clustering heat map revealed that of these differentially expressed proteins, the top 4 upregulated proteins encompassed BGN, PKM, CALR, EIF5A. On the contrary, the top 7 downregulated proteins included COL4A2, CD9, MRC2, ITPR1, C1QTNF3, PGM1, MON1A (Fig. 3B). According to gene ontology (GO) enrichment analysis, the upregulated proteins were implicated in binding, and extracellular region part (Fig. 3C). One of the increased protein Biglycan (BGN), acting as a small leucine-rich repeat proteoglycan, presents in a multitude of extracellular matrix tissues and plays critical roles in structural organization and external signal transduction [28], we then paid close attention to its effect on SHED-sEVs. It was previously established that compared with DPSC-sEVs, the upregulated proteins in the SHED-sEVs included Biglycan, which could activate BMP signaling [29]. Accordingly, in our study, we also validated by the WB assessment that the expression of BGN was enormously augmented in SHED-sEVs (Fig. 3D), consistent with the above bioinformatics analysis.

Young protein BGN activates BMP4 signaling to promote osteogenesis

We further illustrate the promising potential of BGN in recapitulating the normal biological functions of IPDLSCs. BGN has been confirmed as an essential regulator for facilitating osteoblast function. By binding to the BMP receptor type IB, BGN reliably stimulated the BMP signaling pathway, thus contributing to osteoblastic differentiation and bone formation [26]. In this regard, we applied purified BGN to IPDLSCs and discovered the increase of BMP4 at a dose and time dependent manner (Sup Fig. 3a-c). Next, we applied different doses of SHED-sEVs and DPSC-sEVs to IPDLSCs and demonstrated that the protein expression level of BGN and BMP4 was markedly increased, especially with the presence of SHED-sEVs (Fig. 4A, B). Therefore, SHED-sEVs -derived BGN could be considered as a robust osteogenic inductive cargo and give rise to the rescue of osteogenesis capability of IPDLSCs via the initiation of BMP signaling cascade.

To verify SHED-sEVs derived protein function, we prepared 3 siRNA sequences targeting BGN (siBGN) to pretreat SHED. As indicated by RT-PCR,

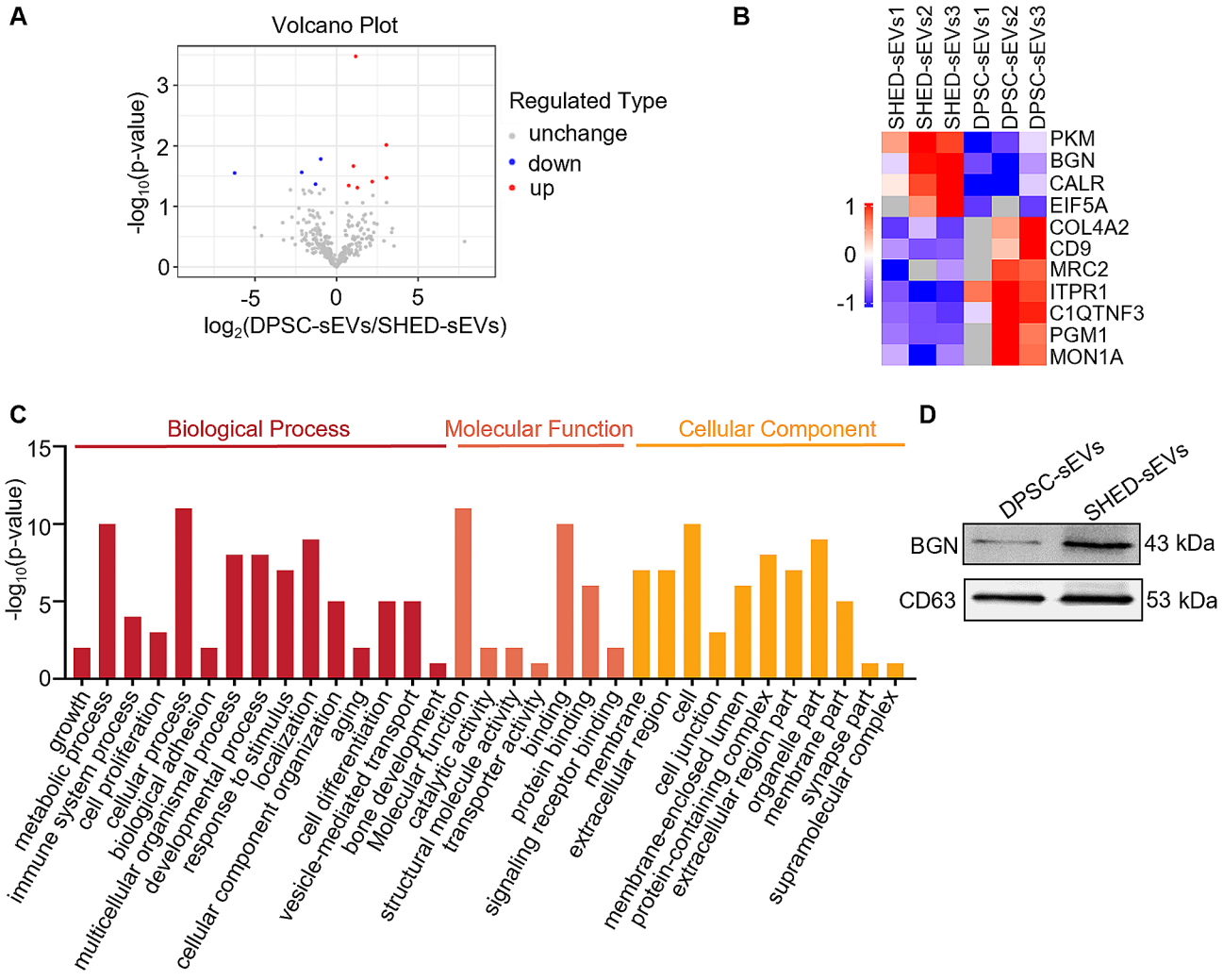

Fig. 3 Proteomics Analysis of differentially expressed proteins in DPSC-sEVs and SHED-sEVs. (**A**) The volcano plot showing differentially expressed proteins between DPSC-sEVs and SHED-sEVs. Red dots: Significantly upregulated proteins. Blue dots: Significantly downregulated proteins. Gray dots: Unchanged proteins. (**B**) The heat map of differentially expressed proteins in DPSC-sEVs and SHED-sEVs. Red color: Relatively high expression of proteins. Blue color: Relatively low expression of proteins. (**C**) Gene ontology (GO) enrichment analysis in DPSC-sEVs and SHED-sEVs. (**D**) As elucidated by WB, the expression of BGN was enormously enhanced in SHED-sEVs compared to DPSC-sEVs

the introduction of siBGN-1, siBGN-2, and siBGN-3 resulted in substantially decreased expression of *BGN* in SHED, among which siBGN-3 elicited a more obvious inhibitory effect (Fig. 4C). In addition, the protein level of BGN in SHED-sEVs was also tremendously suppressed after exposure to siBGN-3 (Fig. 4D), indicating siBGN-3 could effectively inhibit BGN activity. In view of this, we extracted sEVs from siBGN-3-pretreated SHED ($SHED^{siBGN}$-sEVs) and explored their role in IPDLSC osteogenesis. Intriguingly, compared with normal SHED-sEVs, $SHED^{siBGN}$-sEVs drastically eliminated ALP activity in IPDLSCs (Fig. 4E). Moreover, according to ARS staining, as opposed to SHED-sEVs, which considerably promoted the formation of calcified nodules, $SHED^{siBGN}$-sEVs dramatically repressed the deposition of mineral nodules (Fig. 4F). Collectively, our in vitro results verified that young SHED-sEVs not only diminished inflammatory responses of IPDLSCs but also were capable of orchestrating the osteogenic capacity of IPDLSCs by delivering BGN through the activation of BMP signaling pathway, paving the way for investigating their benefits in vivo.

Young SHED-sEVs exhibit anti-inflammatory activity and facilitate infected bone regeneration in vivo

Clinically, chronic apical periodontitis is manifested by alveolar bone destruction and inflammatory granuloma formation. Repairing damaged regions caused by apical periodontitis predominantly depends on the reconstruction of fibrous connective tissue and the formation of new alveolar bone. The complete healing of periapical

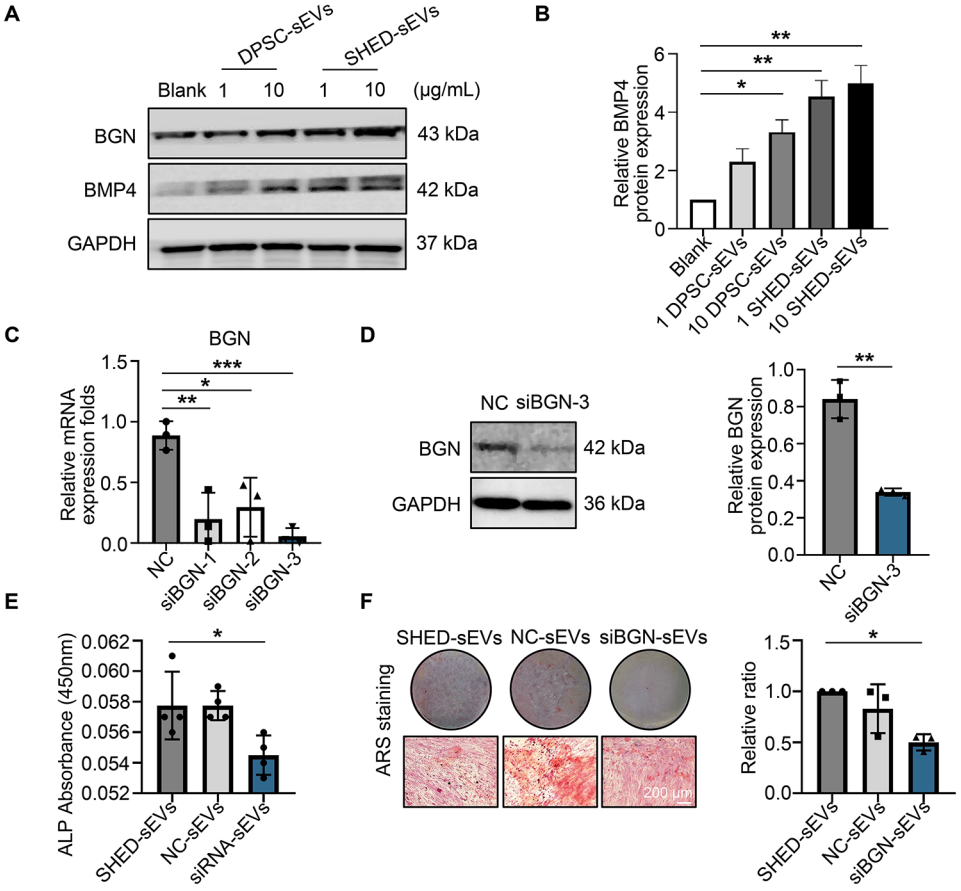

Fig. 4 Knocking down BGN inhibits the anti-inflammatory and osteogenic effects of SHED-sEVs on IPDLSC. (**A**)-(**B**) The protein expression of BGN and BMP4 in IPDLSCs were evaluated by immunoblotting when treated with different dose of sEVs. (**C**) RT-PCR showing the expression of BGN mRNA in SHED treated with NC, siBGN-1, siRNA-2 and siRNA-3 and untreated group ($n=3$). (**D**) Western blot showing the expression level of BGN in SHED derived sEVs treated with control NC and siBGN-3 ($n=3$). (**E**) ALP of IPDLSC cultured on SHED-sEVs, NC-sEVs and siBGN-sEVs for 7 days ($n=4$). (**F**) ARS staining images and quantification of IPDLSC treated with SHED-sEVs, NC-sEVs and siBGN-sEVs for 14 days ($n=3$). Data are presented as mean ± SD; One-way ANOVA was performed for comparisons. *$p<0.05$, **$p<0.01$, ***$p<0.001$

periodontitis lesions is estimated within six months to two years, and some may be more time-consuming [30]. In fact, the host's attempt to promote destroyed tissue remodeling is compromised by the persistent inflammatory responses and attenuated osteogenic potential of surrounding MSCs. To address this issue, we established chronic apical periodontitis models in mouse mandibular first molars to simulate clinical situations with infectious bone defects (Sup Fig. 4) and investigated whether young SHED-sEVs could exhibit anti-inflammatory and pro-osteogenic effects. As depicted in Fig. 5A, the dental pulp was mechanically exposed to the oral environment for 3 weeks to create an infection channel for inducing apical periodontitis. Then, SHED-sEVs and DPSC-sEVs were injected into root canals at 10 μg/mL per week for 2 weeks. By performing micro-CT assessment, we observed that in contrast with PBS, the employment of SHED-sEVs and DPSC-sEVs contributed to inflammation subsidence and reduced volume of periapical bone resorption (Fig. 5B, red area). It was worth noting that SHED-sEVs was more reliable and effective than DPSC-sEVs (Fig. 5C). Additionally, hematoxylin and eosin (H&E) staining revealed that SHED-sEVs and DPSC-sEVs displayed a unique impeding effect on inflammatory cell infiltration and apical alveolar bone resorption (Fig. 5D). Still, SHED-sEVs exhibited better performance than DPSC-sEVs. According to immunohistochemistry staining, higher expression levels of BMP4 and Runx2 were identified for regenerated alveolar bone after applying SHED-sEVs and DPSC-sEVs (Fig. 5E, F), further confirming that SHED-sEVs, as suitable bioactive agents, possessed enormous potential to inhibit periodontitis and promote alveolar bone regeneration.

Aimed at exploring the therapeutic prospects of young SHED-sEVs in facilitating the repair and regeneration of large-scale inflammatory bone defects, we created 3 mm diameter alveolar bone defects in rats at the buccal side of mandibular first molar roots, and 10 μg LPS and LTA were injected around the defect areas (Fig. 6A). sEVs are susceptible to diffusion and

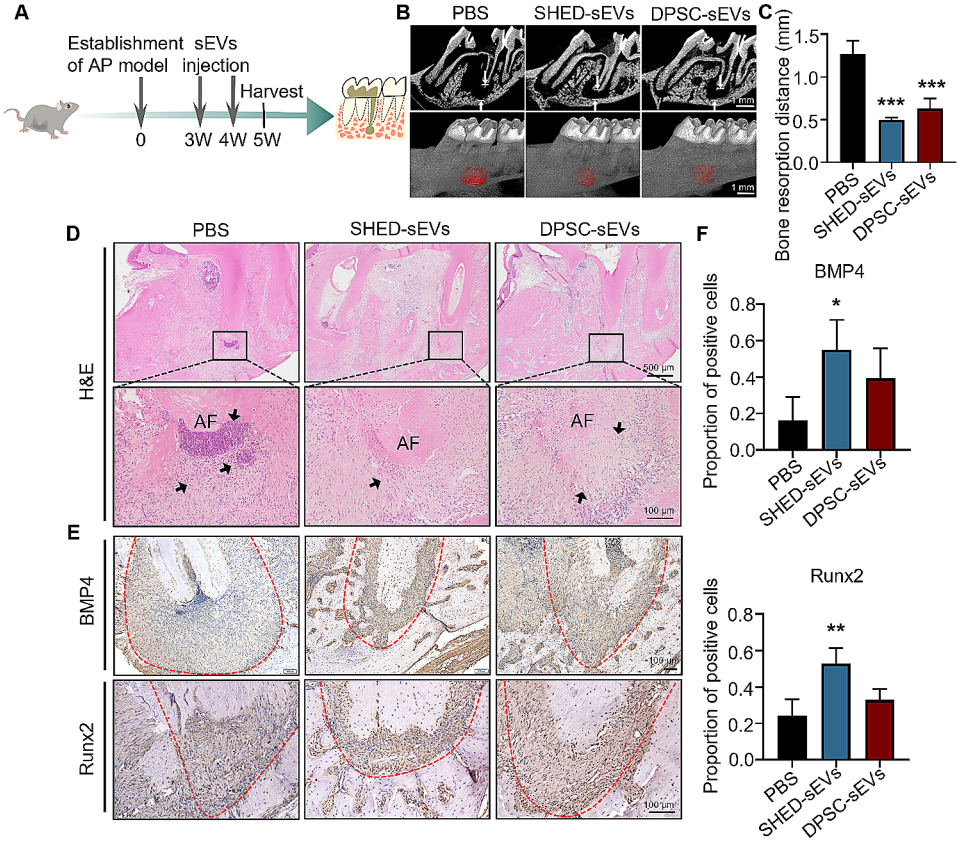

Fig. 5 In vivo periapical inflammation models evidence that SHED-sEVs has more remarkable anti-inflammatory and osteogenic effects. (**A**) Schematic diagram of apical periodontitis model within the mandibular first molar in mice subjected to different treatments through root canal injection of sEVs. (**B**) Representative micro-CT reconstruction images of apical bone defect in the apical periodontitis model. White arrows, periapical distance; red shading, the volume of bone resorption. (**C**) Quantification of distance from apical foramen to alveolar bone ($n = 3$). (**D**) Hematoxylin and eosin images of the apical bone tissues in the defect area. AF, apical foramen. Black arrows, inflammatory area. The black arrows mark the inflammatory cells infiltration areas. (**E**) Immunohistochemistry staining and (**F**) quantitative analysis of BMP4 and Runx2 ($n = 3$). Red dotted line, periapical inflammatory area. Data are presented as mean ± SD; One-way ANOVA was performed for comparisons. $^{*}p < 0.05$, $^{**}p < 0.01$, $^{***}p < 0.001$

might be quickly eliminated by the immune system after injection [31]. It has been investigated that the gel drug delivery system maintains the structure and function of cells or bioactive molecules and improves the delivery efficiency, resulting in better therapeutic efficacy and stronger specificity for tissue damage [32]. We incorporated SHED-sEVs and DPSC-sEVs (20 μg/mL) within commercial hydrogels to enhance sEVs sustainable release while extending their therapeutic efficacy. The release rate of the labeled sEVs showed a controlled release curve during the monitoring time (Sup Fig. 5). As detected by a fluorescence microscope, sEVs labeled with PKH26 were extensively distributed in hydrogels and exhibited a prolonged release for up to 14 days (Fig. 6B), indicating that sEVs maintained structural stability and bioactivity, which provide a solid foundation for exerting long-term efficacy. Subsequently, sEVs embedded in hydrogels were transplanted into bone defect areas, and the bare hydrogels were set up as negative control, while no treated group was designed as blank control. After 14 days, Micro-CT assessment disclosed that SHED-sEVs and DPSC-sEVs could remarkably facilitate new bone formation, which was further verified by significantly elevated BMD and BV/TV (Fig. 6C, D). HE staining showed that the introduction of SHED-sEVs and DPSC-sEVs contributed to the regeneration of large-volume bone-like tissues characterized by vascularized bone marrows and sparse osteocytes embedded in bone lacunas (Fig. 6E). In addition, as suggested by Masson's trichrome staining, sEVs were beneficial for the accumulation of blue-stained collagen matrix (Fig. 6E), further emphasizing the desirable role of SHED-sEVs and DPSC-sEVs in accelerating infected bone regeneration. To ascertain the mechanisms underlying SHED-sEVs-mediated performance, we determined by immunohistochemistry staining that, in contrast with DPSC-sEVs, SHED-sEVs displayed a more robust promoting effect on the expression intensity of BMP4 (Fig. 6F). Consistent with the apical periodontitis

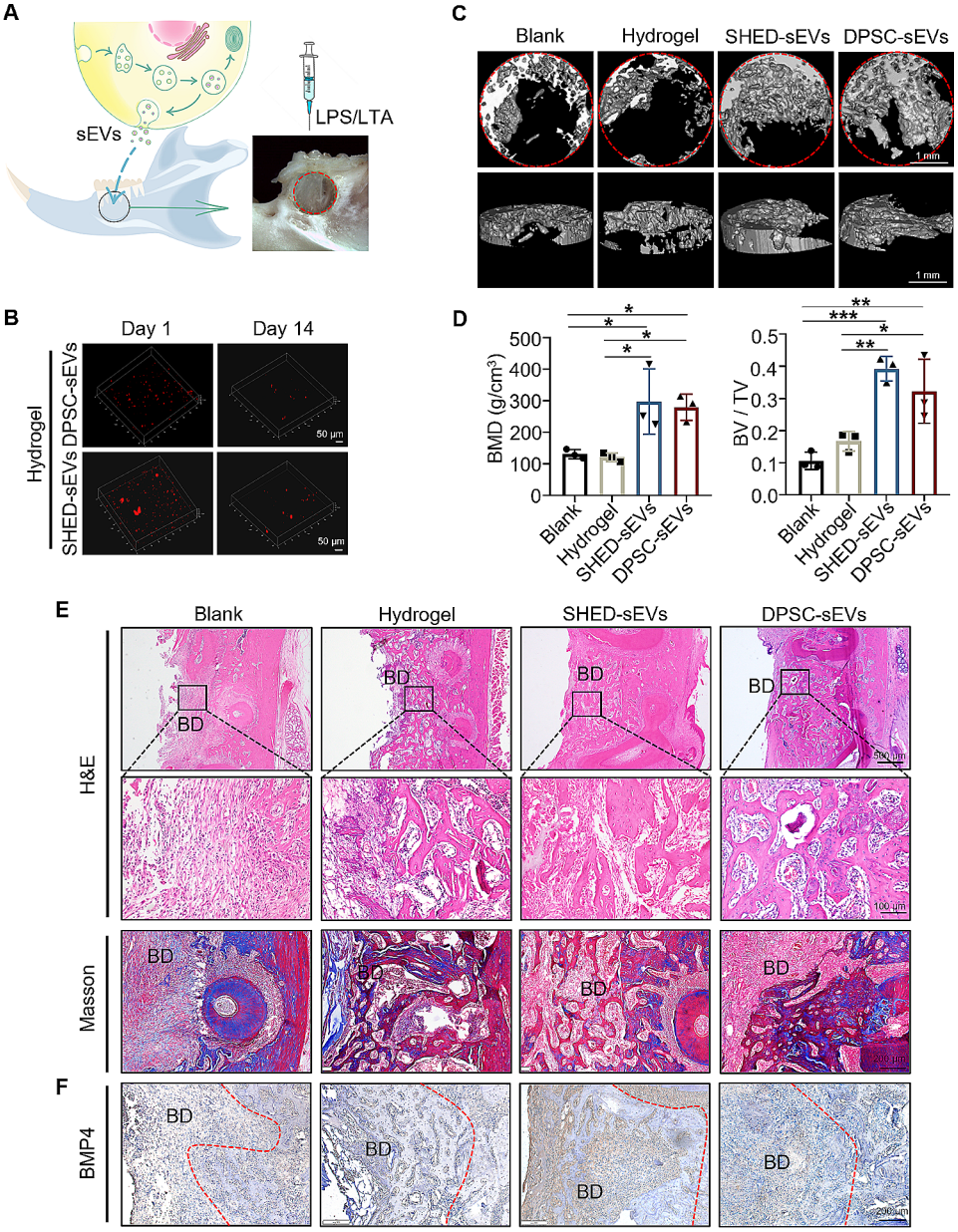

Fig. 6 sEVs enhance infectious alveolar bone defect. (**A**) Schematic illustration showing the induction of infectious bone defect and treatment with applying control-released sEVs. (**B**) Control release of sEVs with hydrogel. Red fluorescent labeled sEVs and hydrogel establish stable complex in 3D images. (**C**-**D**) Micro-CT analysis showed new bone formation and performed quantitative analysis of BMD (g/cm3) and BV/TV amongst groups ($n = 3$). Data are presented as mean ± SD; One-way ANOVA was performed for comparisons. *$p < 0.05$, **$p < 0.01$, ***$p < 0.001$. (**E**) Representative images of HE and Masson staining in alveolar bone defect area. (**F**) Immunohistochemistry staining of BMP4 in the bone defect subjected to different. BD, bone defect; black arrows, new bone formation area; red dotted line: bone defect area

model, SHED-sEVs-loaded hydrogel exhibited superior pro-osteogenesis effects in the large-scale inflammatory bone recovery.

Discussion

Impaired MSCs function has been one of the challenges in the infectious bone regeneration. In this study, a positive role of young sEVs was indicated in the restoration of osteogenesis of inflammatory PDLSCs with the relatively lower dose. It was found that Biglycan expression increased in young sEVs, which was positively associated with BMP4 activation. Functionally, local injection of SHED-sEVs exhibited a favorable MSCs recovery activity and bone regenerative effect in chronic apical periodontitis model in vivo. We further developed SHED-sEVs loaded hydrogel to extend therapeutic intervention for large infective bone defects (Fig. 7). Taken together, based on our in vivo findings, we

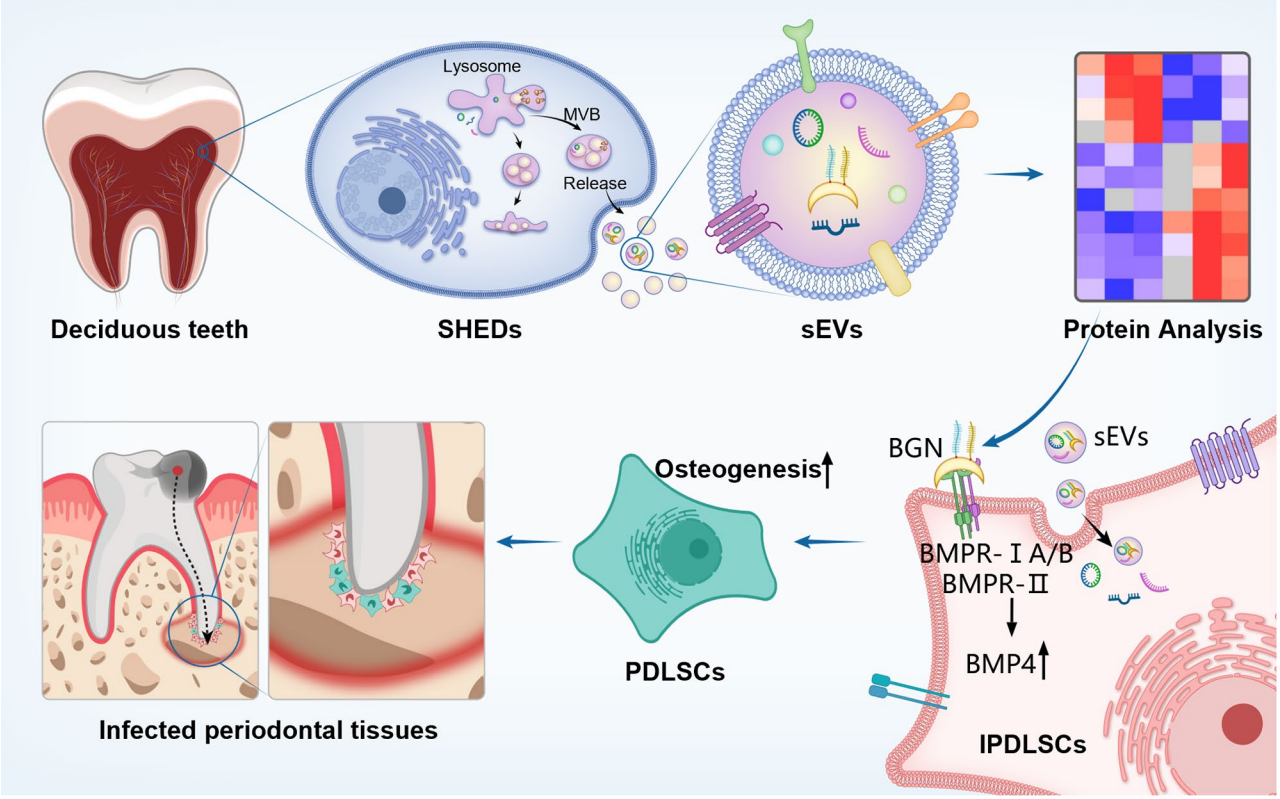

Fig. 7 The schematic illustration of youthful sEVs isolation and protein identification, restoration of mesenchymal stem cells functions and bone repair in vivo

believe that the application of SHED-sEVs will provide promising therapeutic value for attenuating IPDLSCs inflammatory responses and rescuing their osteogenic differentiation potential, therefore enhancing infected bone regeneration.

PDLSCs are periodontal membrane-derived MSCs and present robust self-renewal ability and multipotent differentiation competency. Under normal physiological conditions, PDLSCs account for the regeneration of periodontal ligament and surrounding alveolar bone [33]. Previous studies have clarified that when challenged by inflammatory environment, the differentiation potential of IPDLSCs was markedly inhibited, consequently resulting in poor regeneration of alveolar bone. However, according to Park et al. [34], IPDLSCs could be isolated from inflamed periodontal tissue and retain the regenerative potential for related periodontal ligament and mineralized cementum. Our results also showed that IPDLSCs expressed similar profiles of MSC surface markers and still maintained the lower level of osteogenesis capacity. Accordingly, in response to injury or pathologic conditions, MSCs have been established to be capable of migrating to the defect sites to compensate for the deficient cell amount [35]. In sharp contrast with health counterparts, IPDLSCs have shown higher migratory capacity [34]. Given the above evidences, reversiing the inflammatory profile of IPDLSCs and alleviating their regenerative potential is essential prerequisite for alveolar bone regeneration in clinical settings.

sEVs function is equivalent to that of intercellular messengers and exhibits a significant role in intercellular material through carrying biological molecules that intimately associated with the types of parental cells. Multiple studies have depicted MSC-sEVs occupying critical positions in bone recovery or tissue repair [36]. Compared to MSC-sEVs, young sEVs derived from SHEDs obtain elevated growth factor profiles, pro-angiogenic and superior immunomodulatory effects [37]. In our study, under inflammatory conditions induced by LPS in vitro, SHED-sEVs held tremendous potential to inhibit pro-inflammatory gene levels in IPDLSCs. Furthermore, when subjected to LTA stimulation in vitro, IPDLSCs exhibited a considerably reduced inflammatory performance after receiving DPSC-sEVs and SHED-sEVs, respectively. We further demonstrated the robust osteoinductive potential of SHED-sEVs at the lower concentration, which is in accordance with the effects treated with DPSC-sEVs at a higher concentration. It has been proved that optimum concentration of sEVs is within a threshold. For instance, sEVs less than 1 μg/mL or more than 10 μg/mL did not show obvious improvement of osteogenic differentiation of IPDLSCs [38]. Here, we also

found that SHED-sEVs did not exhibit supreme biological function along with a higher dose treatment. Collectively, these results identify a critical role of sEVs and applying lower dose of young SHED-sEVs (1 μg/mL) exhibited relative robust potential compared to higher dose adult DPSC-sEVs in ameliorating the osteogenesis of IPDLSCs.

Biochemical composition of sEVs contains the specific molecule, such as proteins, nucleic acids and lipids. It was differed due to parent cellular origin and/or conditions under which EVs were generated [39]. Recent investigations demonstrated that young sEVs from plasma could reverse degenerative changes and age-related dysfunction by enhancing mitochondrial energy metabolism [40]. In the current study, we compared protein compositions between the young and adult sEVs and deciphered 4 proteins that accumulated in SHED-sEVs. BGN, a proteoglycan of the small leucine-rich repeat family, is present in all connective tissues and plays key structural and signaling roles. It is one of the major non-collagenous proteins in mineralized tissues and was originally identified in the mineral-associated compartment of bone [41]. It has been found involved in maintaining the mineralization of teeth and bones, the transparency of the eyes, the tensile strength of skin and tendon, the viscoelasticity of blood vessels, and the compressive properties of cartilage [42, 43]. As a positive modulator of osteoblast function, BGN has been found binding to the BMP receptors, which primarily determine the BMP signaling pathway. This pathway is essential for osteoblast differentiation and bone formation, not only in bone development but also in the regeneration processes [28, 44]. In our study, BGN was accumulated in the SHED-sEVs and gave rise to activation of BMP4, which interprets the restoration of osteogenesis ability in the IPDLSCs [45]. In addition to the extensive evidence of BGN role in the bone homeostasis, studies have also looked into BGN function in aging. In mineralized tissue, the level of BGN has been proven to be age-dependent and decreased during aging [46], which is consistent with our mass spectrometry results showing the decrease expression of BGN in adult DPSC-sEVs. The reduction of BGN can affect receptor(s) activation and downstream signaling, leading to age-related deterioration of bone quality [47].

In addition to BGN, the other 3 proteins enriched in SHED-sEVs were related to tissue regeneration, anti-inflammation, and cell aging. Pyruvate kinase M1/2 especially PKM2, are ubiquitously expressed during embryogenesis, tissue regeneration and cancer tissues [48]. Recently, accumulating evidence has illustrated that increased expression of PKM1/2 elicited positive implications on the enhanced pyruvate kinase activity, regulation of mitochondrial function, and cementoblastic differentiation of PDLSCs in an inflammatory environment [49]. The eukaryotic translation initiation factor 5 A (eIF5A) is an evolutionarily conserved protein that participates in proliferation, differentiation, autophagy, apoptosis and aging [50]. In aged cells, the expression of eIF5A was markedly diminished [51]. Consistently, our proteomic results suggested that young sEVs possessed higher level of eIF5A. Regarding that the activation of eIF5A gave rise to the rejuvenation of immune and vascular systems [51], young SHED-sEVs in the present study probably played a critical role under an anti-aging and anti-inflammatory environment. Calreticulin (CALR) is an endoplasmic Ca^{2+} binding protein that participates in a series of cellular processes, such as development heart tissue differentiation and oncogenesis [52]. It has been verified that CALR inhibited inflammation-induced osteoclastogenesis and bone resorption [53], shedding light on their benefits in bone reconstruction. Despite that 7 proteins were delineated to downregulate in SHED-sEVs compared to DPSC-sEVs, some of them were involved in osteogenesis and anti-inflammation processes. For example, COL4A2 was capable of promoting osteogenic differentiation of PDLSCs through negative regulation of Wnt/β-catenin pathway [54]. Reportedly, Mon1a also plays an essential role in the secretion of proteins involved in macrophage immune response [55]. Recently, SHED-sEVs have been proven possessing anti-senescent functions in rescuing aging impaired tendon stem/progenitor cell function and tendon homeostasis [56]. In this case, SHED-sEVs may also serve as an efficient tool for aging related bone regeneration treatment. Despite the identification of proteins in our study, the potential contributions of other biomolecules in sEVs, such as nucleic acids or lipids, contribute to osteogenesis and anti-aging effects require further investigation.

The application of sEVs in vivo is encouraged to consider particles biodistribution and pharmacokinetics to achieve optimal application effect. Recently, intravenous (IV) injection of labelled sEVs into a non-human primate model were detected in the major organs, such as spleen, lung, liver and kidney, after 1 h, and EV circulation times strongly decreased after repeated IV injection, due to immune responses possibly [57]. In contrast to systematically administration, when sEVs are needed to function at specific sites, locally administration is an alternative promising approach. Here, in the chronic apical periodontitis model, apical bone defect area is restricted and sEVs could be applied through root canal channel to limit their diffusion. As a result, we applied sEVs twice per week and observed decease of inflammatory cell infiltration and less bone resorption area due to SHED-sEVs osteo-inductive and anti-inflammation functions. However, when facing to the irregular or large-scale closure bone defect, sEVs are encouraged to be applied with the stable engineered scaffolds. Hydrogel has porous structural properties and good biocompatibility which

serving as optimal sEVs carriers [58]. The engineered sEVs-loaded hydrogel in our study allowed the controlled release of sEVs and prolonged retention time to 14 days. With the modification of hydrogel, the release time of sEVs even can be elongated up to one month [59]. However, we cannot dismiss that some issues need to be further addressed. Firstly, optimal dosing of sEVs with controlled-release system should be tested in vivo since functional sEVs concentration is within a threshold. Secondly, most current studies have addressed biodistribution and pharmacokinetics performance in rodents, but little evidence is available for larger animals, which is necessary to provide guidance for clinical application.

Conclusion

In summary, our study demonstrated that the biological properties of PDLSCs in osteogenic differentiation were significantly impaired by inflammatory stimulus, which could be recovered through the application of sEVs from SHED and DPSC. Youthful sEVs presented a more pronounced effect compared to adult sEVs in promoting the osteogenic differentiation of inflammatory PDLSCs. Mechanically, Biglycan in youthful sEVs efficiently induces osteogenesis by activating BMP4 signaling. Local administration of SHED-sEVs exhibited excellent bone regeneration effects under an inflammatory environment, both in apical periodontitis and massive bone defect animal models. Our research provides the promising therapeutic potential of these sEVs in the field of infectious bone regeneration.

Supplementary Information

The online version contains supplementary material available at https://doi.org/10.1186/s12951-024-02752-6.

Supplementary Material 1

Acknowledgements

This work was supported by the National Natural Science Foundation of China (no. 81970901), Basic Research Program of Shanxi Province project(202303021211127), Natural Science Foundation of Hubei Province (No. 2022CFB717), and Cultivation Project of Tongji Hospital Research Fund (No. 2022B25).

Author contributions

Jiaqi Yang and Junxiang Su conceived the study, performed the experiment and wrote the manuscript. Zhuo Sun, Yeqing Song, Ziqian Zhang and Jizhen Wei performed the experiment. Yimei Zhang and Xin Shi contributed to funding acquisition and reviewed the manuscript. Nan Jiang and Xuejun Ge conceived the study, contributed to funding acquisition and supervision.

Data availability

No datasets were generated or analysed during the current study.

Declarations

Competing interests

The authors declare no competing interests.

Author details

[1]Department of Endodontics, Shanxi Medical University School and Hospital of Stomatology, Taiyuan, Shanxi, China
[2]Central Laboratory, Peking University School and Hospital of Stomatology & National Center for Stomatology & National Clinical Research Center for Oral Diseases & National Engineering Research Center of Oral Biomaterials and Digital Medical Devices, Beijing, China
[3]Department of Stomatology, Shanxi Provincial Cardiovascular Hospital, Taiyuan, Shanxi, China
[4]First Clinic Division, Peking University School and Hospital of Stomatology & National Center for Stomatology & National Clinical Research Center for Oral Diseases & National Engineering Research Center of Oral Biomaterials and Digital Medical Devices, Beijing, China
[5]Center of Stomatology, Tongji Hospital, Tongji Medical College, Huazhong University of Science and Technology, Wuhan, China

Received: 18 April 2024 / Accepted: 2 August 2024
Published online: 24 August 2024

References

1. Han Z, et al. Advances in reparative materials for infectious bone defects and their applications in maxillofacial regions. J Mater Chem B. 2024;12(4):842–71.
2. Ren GH, et al. Treatment options for infected bone defects in the lower extremities: free vascularized fibular graft or Ilizarov bone transport? J Orthop Surg Res. 2020;15(1):439.
3. Deas DE et al. Scaling and root planing vs. conservative surgery in the treatment of chronic periodontitis Periodontol., 2000, 2016;71(1):128-39.
4. Xu XY, et al. Concise Review: Periodontal tissue regeneration using stem cells: strategies and translational considerations. Stem Cells Transl Med. 2019;8(4):392–403.
5. Zhou M, et al. The protective effect of tetrahedral framework nucleic acids on periodontium under inflammatory conditions. Bioact Mater. 2021;6(6):1676–88.
6. Kinane DF, Stathopoulou PG, Papapanou PN. Periodontal diseases. Nat Rev Dis Primers. 2017;3:17038.
7. Seo BM, et al. Investigation of multipotent postnatal stem cells from human periodontal ligament. Lancet. 2004;364(9429):149–55.
8. Zhang Z, et al. Periodontal ligament stem cells in the periodontitis niche: inseparable interactions and mechanisms. J Leukoc Biol. 2021;110(3):565–76.
9. Lin L, et al. UCHL1 impairs Periodontal Ligament Stem Cell Osteogenesis in Periodontitis. J Dent Res. 2023;102(1):61–71.
10. Kalluri R, LeBleu VS. The biology, function, and biomedical applications of exosomes. Science, 2020. 367(6478).
11. Das S, Lyon CJ, Hu T. A Panorama of Extracellular Vesicle Applications: from biomarker detection to therapeutics. ACS Nano; 2024.
12. Barile L, Vassalli G. Exosomes: therapy delivery tools and biomarkers of diseases. Pharmacol Ther. 2017;174:63–78.
13. Zhao Y, et al. Neutrophil membrane-camouflaged Polyprodrug Nanomedicine for inflammation suppression in ischemic stroke therapy. Adv Mater. 2024;36(21):e2311803.
14. Welsh JA, et al. Minimal information for studies of extracellular vesicles (MISEV2023): from basic to advanced approaches. J Extracell Vesicles. 2024;13(2):e12404.
15. van Niel G, D'Angelo G, Raposo G. Shedding light on the cell biology of extracellular vesicles. Nat Rev Mol Cell Biol. 2018;19(4):213–28.
16. Lopez-Otin C, et al. Hallmarks of aging: an expanding universe. Cell. 2023;186(2):243–78.
17. Wang Y et al. Young Sca-1(+) bone marrow stem cell-derived exosomes preserve visual function via the miR-150-5p/MEKK3/JNK/c- Jun pathway to reduce M1 microglial polarization J Nanobiotechnology, 2023. 21(1): p. 194.
18. Miura M, et al. SHED: stem cells from human exfoliated deciduous teeth. Proc Natl Acad Sci USA. 2003;100(10):5807–12.
19. Bar JK, Lis-Nawara A, Grelewski PG. Dental Pulp Stem Cell-Derived Secretome and its regenerative potential. Int J Mol Sci, 2021. 22(21).
20. Du Z, et al. SHED-derived exosomes ameliorate hyposalivation caused by Sjogren's syndrome via Akt/GSK-3beta/Slug-mediated ZO-1 expression. Chin Med J (Engl). 2023;136(21):2596–608.
21. Pivoraite U, et al. Exosomes from Human Dental Pulp Stem cells suppress Carrageenan-Induced Acute inflammation in mice. Inflammation. 2015;38(5):1933–41.

22. Yu T et al. Exosomes miR-92a-3p from human exfoliated deciduous teeth inhibits periodontitis progression via the KLF4/PI3K/AKT pathway J Periodontal Res, 2024.
23. Wu M, et al. SHED aggregate exosomes shuttled miR-26a promote angiogenesis in pulp regeneration via TGF-beta/SMAD2/3 signalling. Cell Prolif. 2021;54(7):e13074.
24. Liu A, et al. Macrophage-derived small extracellular vesicles promote biomimetic mineralized collagen-mediated endogenous bone regeneration. Int J Oral Sci. 2020;12(1):33.
25. Villarroya-Beltri C, et al. ISGylation controls exosome secretion by promoting lysosomal degradation of MVB proteins. Nat Commun. 2016;7:13588.
26. Feng D, et al. Cellular internalization of exosomes occurs through phagocytosis. Traffic. 2010;11(5):675–87.
27. Wang D, et al. Cell membrane vesicles with enriched CXCR4 Display enhances their targeted delivery as Drug Carriers to Inflammatory sites. Adv Sci (Weinh). 2021;8(23):e2101562.
28. Parisuthiman D, et al. Biglycan modulates osteoblast differentiation and matrix mineralization. J Bone Min Res. 2005;20(10):1878–86.
29. Mochida Y, Parisuthiman D, Yamauchi M. Biglycan is a positive modulator of BMP-2 induced osteoblast differentiation. Adv Exp Med Biol. 2006;585:101–13.
30. Siqueira JF Jr., et al. Causes and management of post-treatment apical periodontitis. Br Dent J. 2014;216(6):305–12.
31. Imai T, et al. Macrophage-dependent clearance of systemically administered B16BL6-derived exosomes from the blood circulation in mice. J Extracell Vesicles. 2015;4:26238.
32. Zhang Y, et al. Umbilical mesenchymal stem cell-derived exosome-encapsulated hydrogels accelerate bone repair by enhancing angiogenesis. ACS Appl Mater Interfaces. 2021;13(16):18472–87.
33. Giannobile WV, et al. Biological factors involved in alveolar bone regeneration: Consensus report of Working Group 1 of the 15(th) European Workshop on Periodontology on Bone Regeneration. J Clin Periodontol. 2019;46(Suppl 21):6–11.
34. Park JC, et al. Isolation and characterization of human periodontal ligament (PDL) stem cells (PDLSCs) from the inflamed PDL tissue: in vitro and in vivo evaluations. J Clin Periodontol. 2011;38(8):721–31.
35. Sasaki M, et al. Mesenchymal stem cells are recruited into wounded skin and contribute to wound repair by transdifferentiation into multiple skin cell type. J Immunol. 2008;180(4):2581–7.
36. Padinharayil H, et al. Mesenchymal stem cell-derived exosomes: characteristics and applications in disease pathology and management. Life Sci. 2024;342:122542.
37. Wang M, et al. SHED-derived conditioned exosomes enhance the osteogenic differentiation of PDLSCs via wnt and BMP signaling in vitro. Differentiation. 2020;111:1–11.
38. Lei F, et al. Treatment of inflammatory bone loss in periodontitis by stem cell-derived exosomes. Acta Biomater. 2022;141:333–43.
39. Lehrich BM, Liang Y, Fiandaca MS. Foetal bovine serum influence on in vitro extracellular vesicle analyses. J Extracell Vesicles. 2021;10(3):e12061.
40. Chen X et al. Small extracellular vesicles from young plasma reverse age-related functional declines by improving mitochondrial energy metabolism. Nat Aging, 2024.
41. Fisher LW, et al. Proteoglycans of developing bone. J Biol Chem. 1983;258(10):6588–94.
42. Iozzo RV. Matrix proteoglycans: from molecular design to cellular function. Annu Rev Biochem. 1998;67:609–52.
43. Iozzo RV, Schaefer L. Proteoglycan form and function: a comprehensive nomenclature of proteoglycans. Matrix Biol. 2015;42:11–55.
44. Kawai S, Sugiura T. Characterization of human bone morphogenetic protein (BMP)-4 and –7 gene promoters: activation of BMP promoters by gli, a sonic hedgehog mediator. Bone. 2001;29(1):54–61.
45. Ou M, et al. Bmp2 and Bmp4 accelerate alveolar bone development. Connect Tissue Res. 2015;56(3):204–11.
46. Grzesik WJ, et al. Age-related changes in human bone proteoglycan structure. Impact of osteogenesis imperfecta. J Biol Chem. 2002;277(46):43638–47.
47. Wang X, et al. Age-related deterioration of bone toughness is related to diminishing amount of Matrix glycosaminoglycans (gags). JBMR Plus. 2018;2(3):164–73.
48. Zhang Z, et al. PKM2, function and expression and regulation. Cell Biosci. 2019;9:52.
49. Li X, et al. LncRNA GACAT2 binds with protein PKM1/2 to regulate cell mitochondrial function and cementogenesis in an inflammatory environment. Bone Res. 2022;10(1):29.
50. Barba-Aliaga M, Alepuz P. Role of eIF5A in mitochondrial function. Int J Mol Sci, 2022. 23(3).
51. Luchessi AD, et al. Insights on eukaryotic translation initiation factor 5A (eIF5A) in the brain and aging. Brain Res. 2008;1228:6–13.
52. Fucikova J, et al. Calreticulin and cancer. Cell Res. 2021;31(1):5–16.
53. Fischer CR, et al. Calreticulin inhibits inflammation-induced osteoclastogenesis and bone resorption. J Orthop Res. 2017;35(12):2658–66.
54. Wen Y, et al. COL4A2 in the tissue-specific extracellular matrix plays important role on osteogenic differentiation of periodontal ligament stem cells. Theranostics. 2019;9(15):4265–86.
55. Wang F, et al. Genetic variation in Mon1a affects protein trafficking and modifies macrophage iron loading in mice. Nat Genet. 2007;39(8):1025–32.
56. Jin S, et al. Young Exosome Bio-nanoparticles restore aging-impaired Tendon Stem/Progenitor cell function and reparative capacity. Adv Mater. 2023;35(18):e2211602.
57. Driedonks T et al. Pharmacokinetics and biodistribution of extracellular vesicles administered intravenously and intranasally to Macaca nemestrina. J Extracell Biol, 2022. 1(10).
58. Wang L, et al. Osteoinductive Dental Pulp Stem Cell-Derived Extracellular vesicle-loaded multifunctional hydrogel for bone regeneration. ACS Nano. 2024;18(12):8777–97.
59. Yerneni SS, et al. Controlled release of Exosomes using atom transfer Radical polymerization-based hydrogels. Biomacromolecules. 2022;23(4):1713–22.

Publisher's Note